

Vortex Stretching of Non-premixed, Diluted Hydrogen/Oxygen Flamelets

Wes Hellwig, Xian Shi, William A. Sirignano

Department of Mechanical and Aerospace Engineering, University of California, Irvine, Irvine CA, 92697

January 30, 2024

Abstract

A three-dimensional flamelet model considering vortex stretching with unitary Lewis number is used to simulate diluted hydrogen-oxygen diffusion flames. Non-reacting nitrogen is used as the diluent gas in the fuel stream. Unitary Lewis number provides a common thermal and mass diffusivity from which to create scalar dissipation rate. Both stable and unstable branches of flammability curves (S-curves) are calculated with three vorticity levels and plotted against multiple input and output parameters. The description of the three-dimensional flamelet structure, allowing vorticity and variable density to produce a centrifugal effect, is seen to be necessary for an accurate determination of the water burning rate. Both maximum temperature and integrated water burning rate nearly collapse to a single curve when plotted versus maximum scalar dissipation rate but do not collapse when plotted versus the local maximum strain rate or the ambient strain rate; however, local strain rate and scalar dissipation rate depend strongly on vorticity and ambient strain rate. It is argued that the controlling inputs and natural parameters for a flamelet embedded in a turbulent eddy are the ambient vorticity and strain rate which are thus the natural parameterizing variables as opposed to local strain rate or scalar dissipation rate within the flame zone. Furthermore, established practices of the scaling of velocity derivatives exist in the literature while scaling laws for scalar gradients are sparse and unsubstantiated, further supporting the use of ambient parameterizing quantities.

Keywords: Flamelet; Vorticity; Scalar Dissipation Rate; Three-dimensionality

Information for Colloquium Chairs and Cochairs, Editors, and Reviewers

1) Novelty and Significance Statement

A novel, three-dimensional, rotational flamelet model is formulated with certain constraints from prior models but some new physics. Specifically, it is shown that including vorticity and three-dimensional strain rates in the model changes the ambient and local strain rates at which diffusion flames extinguish. Furthermore, it is shown that scalar dissipation rate depends on vorticity and ambient strain rate and thus cannot be used to distinguish between all possible flame states. This is significant because it provides a basis for which LES and RANS simulations may more accurately predict combustion dynamics.

2) Author Contributions

- *WH: Performed research, analyzed data, and wrote the paper*
- *XS: Analyzed data, edited the paper*
- *WS: Analyzed data, edited the paper*

1. Introduction

Combustion occurring in practical engineering flows is subject to turbulence. In such flows, chemical reactions predominantly occur on the smaller turbulent length scales, within an order of magnitude of the Kolmogorov scale. It is well known that magnitudes of velocity gradients increase with decreasing length and velocity scales because the Kolmogorov length scale, with Reynolds number (Re), behaves as $Re^{-3/4}$, and decays faster than the velocity scale, which behaves as $Re^{-1/4}$. Therefore, the various velocity derivatives, three principal-normal-strain rates and vorticity, impact local flame structure, extinction, and re-ignition.

Past models of such flames are based on the flamelet concept pioneered by Williams [1] which considers turbulent flames existing in the layer between oxidizer and fuel interfaces as an ensemble of thin, highly-sheared, one dimensional, diffusive-reactive zones. The flamelet approximation is governed by the assumption that chemical and diffusive time scales are sufficiently short, such that a quasi-steady assumption can be made for each flamelet. We deal here only with flames on the order of the Kolmogorov scale which have the shortest characteristic length and time so that the quasi-steady assumption is upheld. Of course, flames in turbulent flows can be larger than the smallest eddies [2, 3], subjecting them to turbulent straining. Flames of this type are beyond the scope of this work but have been addressed in the literature [4, 5]. Other non-premixed flame models that have no intrinsic application to turbulence exist, such as the ChemKin OPPDIFF and Cantera difflame codes which solve a counterflow diffusion flame issuing from opposing nozzles [6, 7]. These models are two-dimensional planar or axisymmetric and do not account for strain rates normal to the nozzle axes (transverse strain rates) nor vorticity.

Flamelet models designed for use in turbulent flow simulations commonly make two-dimensional planar or axisymmetric assumptions, allowing the governing system of equations to be reduced to one-dimensional ordinary differential equations (ODEs), and do not include vorticity or transverse strain rates. A transformation to mixture fraction space is commonly made to simplify the computation by removing the chemical source term. In the progress variable approach, upon which many recent flamelet models are based, Pierce and Moin [8, 9] acknowledge that Peters' practice [10, 11] of prescribing counterflow transverse velocity via a fixed strain rate, $u(x) = -S_1^* x$, is not valid across the entire domain as it violates the continuity equation, ignoring important dilatation effects. Pierce and Moin adopt zero advection in its place, and apply Dirichlet boundary conditions to species and enthalpy at a finite separation distance, $y = 0$ and $y = L$ in lieu of solving the momentum equations. This simulates counterflow streams by capping the diffusive domain, creating scalar gradients from which scalar

dissipation rate can be defined. The scalar dissipation rate obtained in this manner is then strongly dependent on the choice of boundary conditions. It is then stated, implicitly or explicitly in models derived from the progress variable approach, that the local flame structure is completely parameterized by maximum scalar dissipation rate and the progress variable.

These models have made great strides simulating turbulent reacting flows, better predicting unsteady flame liftoff; yet, there is still room for improvement by solving the three-dimensional momentum equations with vortex stretching to obtain the velocity field. Unless the momentum equations give the correct velocity, one cannot expect to obtain the correct dZ/dy and thus the correct scalar dissipation rate. We show in this manuscript that vortex stretching is crucial in the solution of the momentum equations and different flame structures exist even for the same scalar dissipation rate.

The present model builds upon two presuppositions regarding the nature of the flow across the length scales. First, there exists in the literature on turbulence, established scaling laws for velocity and velocity derivatives, making these the obvious choices for input parameters. Second, we hypothesize that the flamelet scale solution "sees" these as far-field or ambient conditions such that a three-dimensional picture of velocity, strain rate, and vorticity exists as boundary conditions for the counterflow. We also note the abundance of evidence in the literature, both from experiment and direct numerical simulation that, for turbulent reacting and nonreacting flows, averages for normal strain rates, shear strain rates, and vorticity are important [12–16], but are completely neglected in flamelet modeling.

Sirignano [17, 18] using one-step chemical kinetics and Fickian diffusion, showed that inclusion of vorticity causes a centrifugal effect that increases the flammability limit and reduces the burning rate. When three principal strain rates are included, i.e. neither a planar nor axisymmetric flow, the centrifugal effect is modified by the far-field strain rates' impact on mass efflux.

In this study, we make four primary points: First, scalar dissipation rate depends on vorticity, as does local strain rate. Extinction curves, T_{max} or burning rate versus scalar dissipation rate nearly collapse, but this is a result of plotting outputs against outputs. Second, vorticity increases the ambient strain rate at which a diffusion flame will extinguish. Third, the ambient transverse strain rates (those normal to the inflow axis) also influence the extinction strain rate. Lastly, we argue that scaling laws for velocity gradients are both more substantiated and more representative of the physics than scaling laws for scalar dissipation rate.

2. Methods

2.1. Governing Equations

To incorporate vorticity (ω), a non-Newtonian reference frame is chosen that rotates about the vorticity axis at a rate of $d\theta/dt = \omega/2$. The governing equations for three-dimensional steady flow in this reference frame are listed below where $a_i = \langle x\omega^2/4, y\omega^2/4, 0 \rangle$ is the centrifugal acceleration in the non-Newtonian reference frame. The low Mach number approximation is made to remove terms involving kinetic energy and viscous dissipation.

$$\frac{\partial(\rho u_j)}{\partial x_j} = 0 \quad (1)$$

$$\rho u_j \frac{\partial u_i}{\partial x_j} + \frac{\partial p}{\partial x_i} = \frac{\partial \tau_{ij}}{\partial x_j} + \rho a_i \quad (2)$$

$$\begin{aligned} \frac{\partial(\rho u_j h)}{\partial x_j} + \frac{\partial}{\partial x_j} \sum_{m=1}^N \rho v_m^d Y_m h_m \\ = \frac{\partial}{\partial x_j} \left(\lambda \frac{\partial T}{\partial x_j} \right) - \rho \sum_{m=1}^N h_{f,m} \dot{\omega}_m \end{aligned} \quad (3)$$

$$\frac{\partial(\rho u_j Y_m)}{\partial x_j} + \frac{\partial}{\partial x_j} (\rho Y_m v_m^d) = \rho \dot{\omega}_m \quad (4)$$

In order to define the scalar dissipation rate commonly used in the literature, see Eq. (17), thermal and mass diffusivities for all species are taken to be equal. We assume unitary Lewis number which specifies the diffusivity at each point in the domain according to Eq. (5). Diffusion velocity and diffusion flux are defined according to Eqs. (6-7). Using Taylor series approximations in classical fashion for transverse velocity components in a counterflow, we obtain a similar solution described by ordinary differential equations [17–19].

$$D = \frac{\lambda}{\rho c_p} \quad (5)$$

$$v_m^d = -\frac{1}{Y_m} D \frac{dY_m}{dy} \quad (6)$$

$$J_m = \rho Y_m v_m^d \quad (7)$$

The similarity solution simplifies the solution to Eqs. (1-4), reducing the scalar fields to functions of only the axial coordinate y . In doing so, we do not account for curvature effects. The velocities in the transverse directions, x and z are assumed to be functions of their respective spatial variables and of y according to Eq. (8-9).

$$u_x = S_1 x f_1' \quad (8)$$

$$u_z = S_2 z f_2' \quad (9)$$

The two constants S_1 and S_2 are the far-field strain rates at $x = +\infty$ and $z = +\infty$, respectively, non-dimensionalized by the ambient strain rate at $y = +\infty$, S^* . For the remainder of this manuscript, * indicates a dimensional quantity. All other quantities are non-dimensional. Variables f_1' and f_2' are two of three similarity variables, all of which are functions of

y only. The third similarity variable is defined according to Eq. (10) from which the v velocity component is found via Eq. (11).

$$f = S_1 f_1 + S_2 f_2 \quad (10)$$

$$u_y = -\frac{f}{\rho} \quad (11)$$

Employing a Howarth–Dorodnitsyn transformation from $y \rightarrow \eta$ allows the equations to be further simplified. For a complete derivation of the similarity solution, the reader is encouraged to see Sirignano [17] pg. A21-11-16. The similar form of the governing equations is presented below along with the equation of state. Equations (12-13) are the momentum equations in the x and z directions. The y momentum equation is not needed to obtain the velocity field but can be used to obtain the pressure gradient.

$$\begin{aligned} \rho \mu f_1''' + f_1''(\rho \mu)' + f f_1'' + S_1 \left(\frac{1}{\rho} - (f_1')^2 \right) \\ + \frac{\omega^2}{4S_1} \left(1 - \frac{1}{\rho} \right) = 0 \end{aligned} \quad (12)$$

$$\rho \mu f_2''' + f_2''(\rho \mu)' + f f_2'' + S_2 \left(\frac{1}{\rho} - (f_2')^2 \right) = 0 \quad (13)$$

$$c_p f T' + (\rho \lambda T')' - T' \sum_{m=1}^N J_m c_{p,m} - \sum_{m=1}^N h_m^0 \dot{\omega}_m = 0 \quad (14)$$

$$f Y_m' - J_m' + \dot{\omega}_m = 0 ; \quad m = 1, 2, 3, \dots, N \quad (15)$$

$$P = \rho R_{sp} T \quad (16)$$

Realize that enstrophy, $\omega^{*2} = \omega^* \cdot \omega^*$ is actually the relevant variable. The direction of rotation in the $x - y$ plane is not relevant. Analytical and experimental studies relate enstrophy to the square of strain rate, concluding that they are of the same order of magnitude [20–22]. As such, we choose to normalize vorticity by normal compressive strain rate, keeping this nondimensional vorticity of $O(1)$; $0 \leq \omega = \omega^*/S^* \leq \sqrt{1.5}$.

The key difference between our flamelet configuration and former models is that our geometry is three-dimensional. Specifically, three normal strain rates are allowed to differ and vorticity can be applied. Furthermore, we do not use a nozzle-counterflow as many opposed-flow flame solvers do. At infinity, we take a potential counterflow which removes the imposition of zero velocity gradients at a fixed nozzle separation distance. Through the similarity solution, this three-dimensional geometry may be solved with ODEs.

2.2. Scalar Dissipation Rate and Mixture Fraction

Instead of strain rate, scalar dissipation rate, χ , is commonly used to classify extinction in flamelet modeling. Beginning with Eq. (18), conservation of mixture fraction Z , an ODE for scalar dissipation rate (SDR) can be derived in terms of the similarity variable f and other quantities known once Eq. (12-16) have been solved. The resultant equation, Eq. (19), is a linear, homogeneous ODE with known boundary conditions, when formulated in terms of the mixture fraction which varies between 0 and 1.

$$\chi \equiv 2D \left(\frac{\partial Z}{\partial x_i} \right)^2 = 2D \left(\frac{dZ}{dy} \right)^2 \quad (17)$$

$$\rho u_y \frac{dZ}{dy} = \frac{d}{dy} \left(\rho D \frac{dZ}{dy} \right) \quad (18)$$

Multiplication by $2(dZ/dy)$ results in a first-order ODE for SDR.

$$\left[\frac{2f}{\rho D} + \frac{2}{\rho D} \frac{d(\rho D)}{dy} - \frac{1}{D} \frac{dD}{dy} \right] \chi + \frac{d\chi}{dy} = 0 \quad (19)$$

By defining C as the constant of integration in Eq. (19) and integrating, Eq. (20) is found for χ .

$$\chi = \frac{C}{\rho^2 D} \exp \left(-2 \int_0^\eta \frac{f}{\rho^2 D} d\eta' \right) \quad (20)$$

Replacing χ in Eq. (20) with $2D(dZ/dy)^2$ through the definition of SDR and integrating from $-\infty \rightarrow \infty$ in η -space such that Z varies from $0 \rightarrow 1$, C is determined.

$$C = \frac{2}{\left(\int_{-\infty}^{\infty} \frac{1}{\rho^2 D} \exp \left[- \int_0^\eta \frac{f}{\rho^2 D} d\eta' \right] d\eta \right)^2} \quad (21)$$

2.3. Chemical Kinetics Model

Multi-step chemical kinetics were incorporated through Cantera [7]. A skeletal version of the Foundational Fuel Chemistry Model 1.0 (ffcm-1) [23] for hydrogen-oxygen combustion was used. This model also includes nitrogen as a non-reacting species for a total of 9 species and 25 reactions. The skeletal model was chosen to decrease computation time.

3. Results

3.1. Equal Transverse Strain Rates ($S_1 = S_2$)

The counterflow diffusion flame studied in the following sections has oxygen (O_2) at 300 K issuing from the left and an equimolar mixture of hydrogen (H_2) and nitrogen (N_2), also at 300 K, issuing from the right. The pressure is set at 10 atmospheres. Calculations were performed for three values of non-dimensional vorticity, $\omega = 0, 1, \sqrt{1.5}$, with $S_1 = S_2 = 1/2$ to simulate the existing flamelet models'

assumption of axisymmetry. Note that our calculations are only axisymmetric when $S_1 = S_2 = 1/2$ and $\omega_k = 0$. When $\omega > 0$, vortex stretching implies non-symmetric behavior.

First, extinction curves, or S-curves, were calculated to determine the flammability limits at each value of ω . Figure 1a shows these extinction curves plotted in three ways from left to right: against the maximum SDR, χ_{max} , the ambient (i.e., inflow) axial strain rate at $y = +\infty$, S^* , and the maximum or local axial strain rate in the flame zone, S_{local}^* .

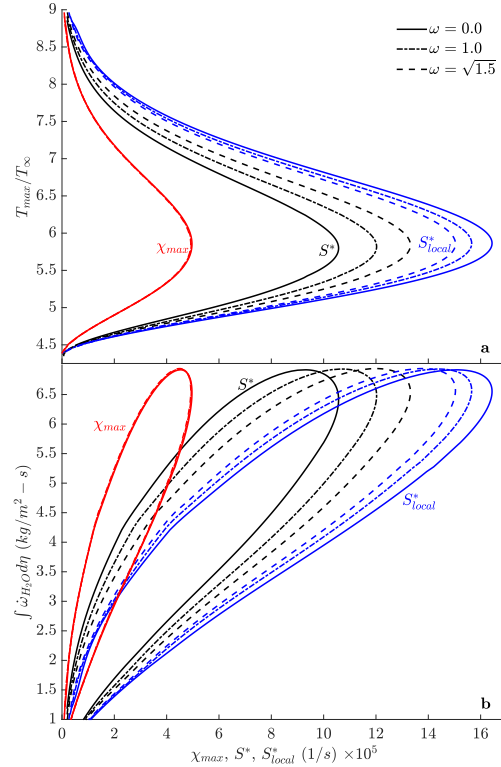


Fig. 1: Extinction curves versus: maximum scalar dissipation rate, χ_{max} (red); ambient strain rate, S^* (black); maximum local strain rate, S_{local}^* (blue).

The black curves show a substantial impact of vorticity on the extinction ambient strain rate of the flames with a 26% increase occurring between $\omega = 0 \rightarrow \sqrt{1.5}$. When local maximum strain rate is used on the abscissa (blue curves), those with $\omega \neq 0$ fall to the left of that with $\omega = 0$ because vorticity-induced changes to the velocity field decrease local strain rate with increasing vorticity. Since the temperature at the extinction point is nearly unchanged by vorticity, those curves with decreased local strain rate fall to the right with increasing vorticity when plotted against the inflow strain rate. When the S-curve is plotted versus maximum SDR, a near-total collapse occurs, although the order of curves follows those versus maximum local strain rate. Figure 1b plots the

integrated burning rate of water (H_2O) along the S -curves in Fig. 1a. Again, the solution is highly dependent on vorticity magnitude when plotted versus S^* and S_{local}^* and significantly collapses versus χ_{max} . Actually, maximum temperature is a better predictor than SDR to capture “collapse”. From Fig. 1, we see that one value of ω together with one value of S^* , S_{local}^* , or χ_{max} determines two values of T_{max} and H_2O burning rate. However, one value of T_{max} with one value of ω gives distinct values for S^* , S_{local}^* , χ_{max} , and H_2O burning rate.

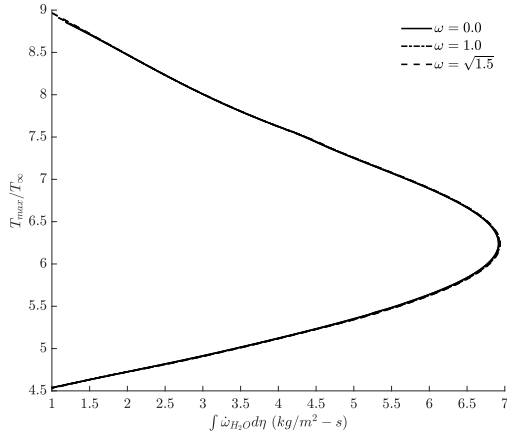


Fig. 2: Temperature versus integrated H_2O burning rate.

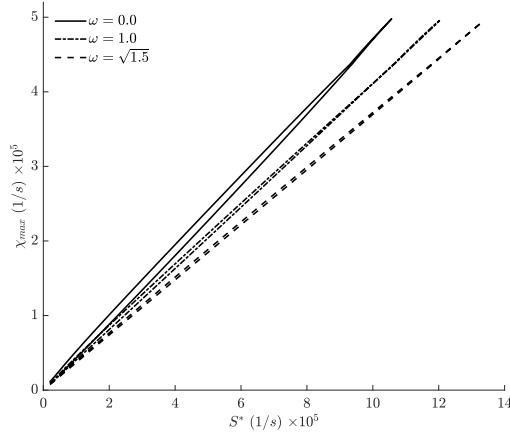


Fig. 3: SDR versus Ambient Strain Rate

If output parameters are plotted versus output parameters, curves with varying vorticities collapse; see Fig. 2 and Fig. 1 (red). However, no output parameters plotted versus the two input parameters, S^* and ω , collapse; see Fig. 3 and Fig. 1 (black, blue).

The tendency of curves to collapse might at first appear convenient, allowing solutions to be parameterized by χ_{max} instead of S^* and ω ; however, some issues persist. At the fundamental level, SDR precludes preferential (unequal Lewis numbers) and differential (non-unitary Lewis numbers) diffusion [24]

since its definition stipulates a common diffusivity. Incorporating detailed transport allows species and heat to locally re-distribute which notably impacts laminar flames [25, 26]. Corrections to models assuming constant Lewis number can be made to better capture the tendencies of differential diffusion [27] but it becomes difficult to create a useful and clearly understood conserved scalar. An alternate approach, governing a conserved scalar with a transport equation in which the diffusivity is equal to the thermal diffusivity but differs from the species diffusivity, was introduced by Pitsch and Peters [28]. Although it is named the “mixture fraction,” it differs from the classical definition and has no clear physical meaning. A very cumbersome set of differential equations are yielded, resulting in a scalar dissipation rate that also has no clear physical interpretation.

Furthermore, in application of a flamelet model to turbulent combustion, the cascades of length, velocity, and velocity derivatives (strain rate and vorticity) are much better understood than the cascades of scalar gradients [29]. So, scaling laws for contrived variables like SDR have little physical basis. Therefore, for several reasons, SDR is not the best choice to characterize flamelet structure and its response to the surrounding flow as determined by the strain rate and vorticity of the inflow. However, employing strain rate and vorticity adds an additional matrix parameter and is thus computationally more expensive.

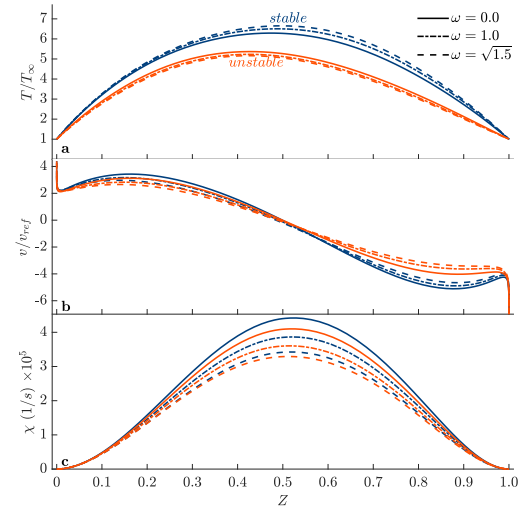


Fig. 4: Temperature and axial velocity versus mixture fraction. Stable branch (navy); unstable branch (orange). $S^* = 903, 500$ 1/s.

The importance of solving the momentum equations with vorticity is illustrated in Fig. 4. Although the velocity curves have the same ambient strain rate, $S^* = 903,500$ 1/s, their slopes and magnitudes differ as a result of mass efflux changes caused by the centrifugal action of vorticity coupled with the density gradients throughout the counterflow. With vor-

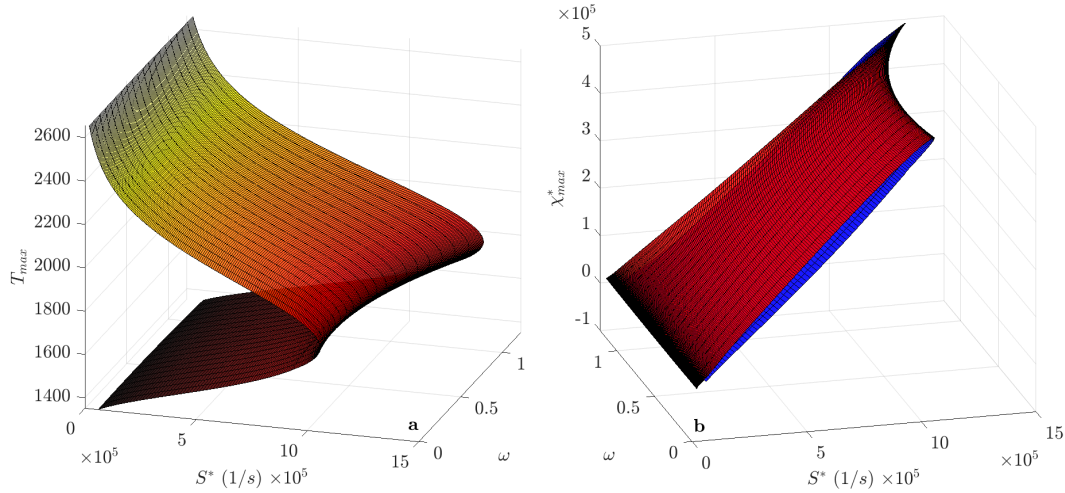


Fig. 5: Three-dimensional extinction surface (a) and SDR surface (b). Subfigure a: temperature color code (dark red \rightarrow red \rightarrow yellow); Subfigure b: stable/unstable branch color code (stable: red; unstable: blue).

ticity, the lighter fluid (products of combustion) tends to flow outward aligned with the vorticity axis as this direction does not experience centrifugal force. The denser fluid is thrown outward in the plane normal to the vorticity axis, counteracting the incoming pressure gradient. This results in a lower strain rate at the stagnation point and thus increased residence time, which is responsible for increased temperatures on the stable branch. Opposite to temperature, SDR decreases as vorticity increases because the lower velocity gradients cause lower mixture fraction gradients. This result, shown in Fig. 4c, clearly indicates that vorticity must be considered to accurately determine SDR. The existing progress variable method relies on taking scalar values at the point of stoichiometric mixture fraction to define the progress variable and parameterize the S-curve [9]. These scalars are typically the temperature, SDR, and a group of specific mass fractions. We show here that such values depend on ω and S^* and should not be viewed as being characterized by one progress variable.

With a wide range of vorticity magnitudes, a three-dimensional surface can be created giving any output parameter as a function of the two input parameters, vorticity (ω) and ambient compressive strain rate (S^*). Figure 5 shows two representations of these surfaces for maximum temperature and scalar dissipation rate by parabolic fitting of the three vorticity cases; $\omega = 0, 1, \sqrt{1.5}$. If viewed in the T_{max} - S^* plane, Fig. 5a appears as the black curves in Fig. 1a and Fig. 5b appears as Fig. 3. These surface plots are given to illustrate the three-dimensional character of the rotational flamelet solutions.

Convergence of the numerical scheme stipulates a less than one percent change in dependent variables between successive Newton iterations, except for minor species mass fractions which show greater volatility. Due to convergence difficulty especially near the extinction limit, the data in Fig. 1-3 and Fig. 5-7 has

been post-processed to achieve smooth transitions between the stable and unstable branches. The associated error with these curve fits is less than 0.5%.

3.2. Unequal Transverse Strain Rates ($S_1 \neq S_2$) and Non-constant Lewis Number

The theory presented in this manuscript is not limited to the assumption of unitary Lewis number or even constant Lewis number. The Fickian diffusion formulation assumed prior, can be replaced by the mixture-averaged or multicomponent diffusion formulation, as was done by Hellwig et al. [19]. These are more accurate diffusion models in which the diffusivities for different species are unique and diffusion velocity depends on the gradients of multiple species. Both diffusion formulations are built on standard kinetic theory although simplifying ad hoc assumptions are made in the mixture-averaged form.

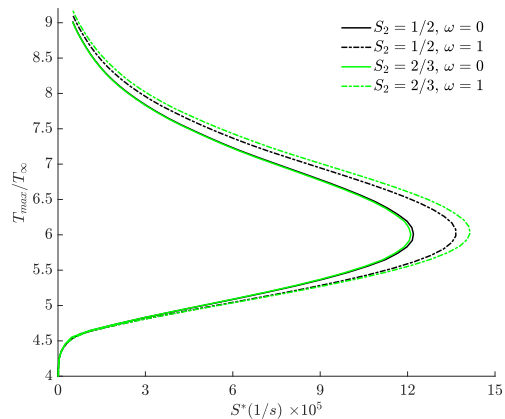


Fig. 6: S-curves using multicomponent diffusion with transverse ambient strain rate variation.

ω	S_1, S_2	S^* (1/s)	$S_1 S^*$ (1/s)	T_{max} (K)	$\int \dot{\omega}_{H_2O} d\eta$ (kg/m ² s)	χ_{max} (1/s)
0	1/2, 1/2	660,000	330,000	2010.5	6.4088	332,350
0	1/3, 2/3	1,000,000	330,000	1817.1	6.8295	483,980
1	1/2, 1/2	800,000	400,000	1996.0	6.5094	344,740
1	1/3, 2/3	1,200,000	400,000	1813.2	6.8434	482,590

Using a multicomponent or mixture-averaged diffusion formulation allows preferential and differential diffusion which breaks two commonly used practices in many flamelet theories: first, scalar dissipation rate is no longer clearly defined since the mass diffusivities of each species are different; secondly, counter-gradient diffusion becomes a possibility, especially if high molecular weight fuels are considered, making the mixture fraction no longer vary monotonically between the oxidizer and fuel inflows which prevents the traditional method of solving the problem in mixture fraction space.

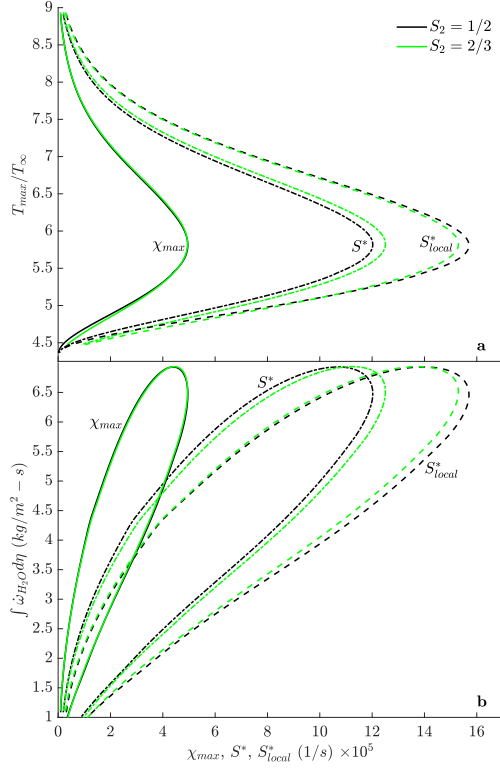


Fig. 7: Extinction curves versus: maximum scalar dissipation rate, χ_{max} ; ambient strain rate, S^* ; maximum local strain rate, S_{local}^* . Vorticity is constant, $\omega = 1$, for all curves. $S_1 = 1/2, 1/3, S_2 = 1/2, 2/3$.

The data for Fig. 6 is taken from [19] and shows S-curves similar to Fig. 1a for $S_1 = S_2 = 1/2$ and $S_1 = 1/3, S_2 = 2/3$ using multicomponent diffusion. Of course, SDR does not appear on the abscissa since it is now undefined. Figure 7 shows a repeat of certain data in Fig. 1 ($Le = 1$); however, vortic-

ity is fixed at $\omega = 1$, while S_1 and S_2 vary. Here again, $S_1 = S_2 = 1/2$ and $S_1 = 1/3, S_2 = 2/3$. These figures illustrate two points. First, the qualitative impact of vorticity on extinction limits is common among constant and variable Lewis number formulations. Secondly, the three-dimensional character of the inflows (magnitudes of S_1 and S_2) alters the extinction limits. With vorticity, a higher transverse strain rate aligned with the vorticity vector, S_2 , yields a more stable flame for a given ambient compressive strain rate, S^* . This occurs because vorticity favors expulsion of low-density fluid outward in the direction unimpacted by centrifugal force, i.e., the direction with which S_2 and ω are aligned.

The original flamelet formulation, using SDR as formulated by Peters [10] (see p. 181-184 of [11]), applies a constant transverse strain rate in the x direction. This strain rate corresponds to our S_1 only at $x = +\infty$ since our transverse strain rates vary with their respective axes and with y . Nevertheless, if two cases are compared in which the transverse strain rate in the x directions are equal, that is $S_1 S^*$ is the same value for two cases, we find peak temperatures differ by $\sim 10\%$, burning rates differ by $\sim 5-6\%$, and maximum SDR differs by $\sim 40-45\%$. Thus, it is clear that the assumptions of constant strain rates and potential flow omit certain physical behaviors that are possible to capture and should be captured.

4. Conclusion

The analysis is built on two hypotheses. First, the flamelet field within the counterflow is determined by the ambient scalar and velocity fields of the two incoming flows. This hypothesis is supported by the analytical results which show that the scalar properties, normal strain rates, and vorticity are influential parameters (to be precise, enstrophy (ω^{*2}) is the parameter that appears in the analysis). Second, these ambient properties are better suited for scaling relations with a resolved flow in a turbulent combustion analysis.

Depending on these inflow conditions, the analysis shows particular three-dimensional spatial variations through the counterflow for the velocity and one-dimensional variation for the scalar properties: e.g., temperature, mass fractions, and SDR. Both a stable branch and an unstable branch are described with different property variations. Thus, two different spatial profiles and values of maximum temperature and integrated burning rate can appear for the same set of ambient conditions. However, nearly the same maximum scalar dissipation rate and the same max-

imum local strain rate or integrated burning rate can appear on both branches. The maximum temperature is a more distinctive single parameter in distinguishing between the two branches.

For a given set of input parameters, the introduction of vorticity and varying transverse strain rates significantly changes the velocity profiles and scalar gradients within the domain. Furthermore, the ambient strain rate at which the flame extinguishes may be increased as much as 26% by vorticity.

Existing flamelet theories neglect the use of vorticity and ambient inflow normal strain rates as critical input parameters [11, 28, 30, 31]. Instead, together with pressure, local conditions at the flame are used for input to the analysis. Specifically, mixture fraction, local normal strain rate and SDR are used to identify all flame characteristics.

The identification of maximum SDR (usually assumed as a Gaussian variation) is claimed to allow identification of the important flame characteristics including burning rate and maximum temperature in many existing flamelet models. On the contrary, our results show that SDR and local strain rate depend strongly on vorticity and inflow strain rate, including how strain rate distributes in a three-dimensional flame structure. Thus, SDR cannot be used to distinguish between all possible flame states. In addition to this problem of major omission of existing theory, there is little literature that can guide the scaling of scalar gradients or SDR from the resolved scale for RANS or LES to the sub-grid scale of the flamelet. SDR is essentially impossible to scale because it asymptotes to zero outside the flamelet. The scaling of vorticity or ambient (inflow) strain rate in turbulent flows is better understood and even is discussed in textbooks. Finally, the use of SDR in flow media with preferential diffusion is highly artificial and controversial. It is clear that a method relying on the scaling of inflow conditions for vorticity and normal strain rate is superior in its analytical foundations and in its ability to apply with models using more detailed transport. Namely, the physics are better described in both qualitative and quantitative terms.

Declaration of competing interest

The authors declare that they have no known competing financial interests or personal relationships that could have appeared to influence the work reported in this paper.

Acknowledgments

The research was supported by the Air Force Office of Scientific Research through Grant FA9550-22-1-0191 with Dr. Justin Koo as program manager and by the Office of Naval Research through Grant N00014-21-1-2467 with Dr. Steven Martens as program manager.

References

- [1] F. A. Williams, Recent advances in theoretical descriptions of turbulent diffusion flames, in: *Turbulent Mixing in Nonreactive and Reactive Flows*, Editor S. N. B. Murthy, Springer, 1975, pp. 189–208.
- [2] M. Dunn, A. Masri, R. Bilger, R. Barlow, G.-H. Wang, The compositional structure of highly turbulent piloted premixed flames issuing into a hot coflow, *Proceedings of the Combustion Institute* 32 (2) (2009) 1779–1786.
- [3] M. Dunn, A. Masri, R. Bilger, A new piloted premixed jet burner to study strong finite-rate chemistry effects, *Combustion and Flame* 151 (1) (2007) 46–60.
- [4] T. Poinsot, D. Veynante, S. Candel, Diagrams of premixed turbulent combustion based on direct simulation, *Symposium (International) on Combustion* 23 (1) (1991) 613–619, twenty-Third Symposium (International) on Combustion.
- [5] O. Colin, F. Ducros, D. Veynante, T. Poinsot, A thickened flame model for large eddy simulations of turbulent premixed combustion, *Physics of Fluids* 12 (7) (2000) 1843–1863.
- [6] ANSYS Chemkin-Pro Theory Manual, ANSYS, Inc., 2021.
- [7] D. Goodwin, H. Moffat, I. Schoegl, R. Speth, B. Weber, Cantera: An object-oriented software toolkit for chemical kinetics, thermodynamics, and transport processes, <https://www.cantera.org>, version 2.6.0 (2022). doi:10.5281/zenodo.6387882.
- [8] C. Pierce, Progress-variable approach for large-eddy simulation of turbulent combustion, Ph.D. Thesis, Stanford University, Stanford, CA, USA (2001).
- [9] C. Pierce, P. Moin, Progress-variable approach for large-eddy simulation of non-premixed turbulent combustion, *Journal of Fluid Mechanics* 504 (2004) 73–97.
- [10] N. Peters, Laminar diffusion flamelet models in non-premixed turbulent combustion, *Progress in Energy and Combustion Science* 10 (3) (1984) 319–339.
- [11] N. Peters, *Turbulent Combustion*, Cambridge University Press, Cambridge U.K., 2000.
- [12] K. Nomura, S. Elghobashi, Mixing characteristics of an inhomogeneous scalar in isotropic and homogeneous sheared turbulence, *Physics of Fluids A* 4 (1992) 606–625.
- [13] K. Nomura, S. Elghobashi, The structure of inhomogeneous turbulence in variable density nonpremixed flames, *Theoretical and Computational Fluid Dynamics* 5 (1993) 153–175.
- [14] O. Boratav, S. Elghobashi, R. Zhong, On the alignment of the a-strain and vorticity in turbulent nonpremixed flames, *Physics of Fluids* 8 (1996) 2251–53.
- [15] O. Boratav, S. Elghobashi, R. Zhong, On the alignment of strain, vorticity and scalar gradient in turbulent, buoyant, nonpremixed flames, *Physics of Fluids* 10 (1998) 2260–67.
- [16] W. Ashurst, A. Kerstein, R. Kerr, C. Gibson, Alignment of vorticity and scalar gradient with strain rate in simulated navier–stokes turbulence, *Physics of Fluids* 30 (1987) 2343–2353.
- [17] W. Sirignano, Three-dimensional, rotational flamelet closure model with two-way coupling, *Journal of Fluid Mechanics* 945 (2022) A21.
- [18] W. Sirignano, Inward swirling flamelet model, *Combustion Theory and Modelling* 26 (2022) 1014–1040.
- [19] W. Hellwig, X. Shi, W. A. Sirignano, Three-dimensional vorticity effects on extinction behavior of laminar flamelets (2023). arXiv:2307.03695.
- [20] R. Betchov, An inequality concerning the production of vorticity in isotropic turbulence, *Journal of Fluid*

- Mechanics 1 (1956) 497–504.
- [21] F. Raynal, Exact relation between spatial mean enstrophy and dissipation in confined incompressible flows, *Physics of Fluids* 8 (8) (1996) 2242–2244. doi: 10.1063/1.868997.
 - [22] Y. Zhu, R. A. Antonia, On the correlation between enstrophy and energy dissipation rate in a turbulent wake, *Applied Scientific Research* 57 (3–4) (1996) 337–347. doi: 10.1007/bf02506068.
 - [23] G. Smith, Y. Tao, H. Wang, Foundational fuel chemistry model version 1.0 (ffcm-1) (2016). URL <http://nanoenergy.stanford.edu/ffcm1>
 - [24] M. Matalon, Intrinsic flame instabilities in premixed and nonpremixed combustion, *Annual Review of Fluid Mechanics* 39 (1) (2007) 163–191.
 - [25] X. Jiang, J. Guo, Z. Wei, E. Quadarella, H. G. Im, Z. Liu, A species-weighted flamelet/progress variable model with differential diffusion effects for oxy-fuel jet flames, *Combustion and Flame* 251 (2023) 112674.
 - [26] A. Donini, R. Bastiaans, J. van Oijen, L. de Goey, Differential diffusion effects inclusion with flamelet generated manifold for the modeling of stratified premixed cooled flames, *Proceedings of the Combustion Institute* 35 (1) (2015) 831–837.
 - [27] S. Gupta, S. Keum, P. Pal, H. G. Im, Modeling of scalar dissipation rates in flamelet models for low temperature combustion engine simulations, *arXiv e-prints* (2014) arXiv:1412.4285arXiv:1412.4285, doi: 10.48550/arXiv.1412.4285.
 - [28] H. Pitsch, N. Peters, A consistent flamelet formulation for non-premixed combustion considering differential diffusion effects, *Combustion and Flame* 114 (1) (1998) 26–40.
 - [29] P. L. Johnson, M. Wilczek, Multiscale velocity gradients in turbulence, *Annual Review of Fluid Mechanics* 56 (1) (2024) 463–490. doi:10.1146/annurev-fluid-121021-031431.
 - [30] M. E. Mueller, Physically-derived reduced-order manifold-based modeling for multi-modal turbulent combustion, *Combustion and Flame* 214 (2020) 287–305.
 - [31] H. Pitsch, M. Ihme, An unsteady/flamelet progress variable method for les of nonpremixed turbulent combustion, in: *Proceedings of the 43rd AIAA Aerospace Sciences Meeting and Exhibit, AIAA, 2005*. doi: 10.2514/6.2005-557.